

JAAS

Accepted Manuscript



This is an *Accepted Manuscript*, which has been through the Royal Society of Chemistry peer review process and has been accepted for publication.

Accepted Manuscripts are published online shortly after acceptance, before technical editing, formatting and proof reading. Using this free service, authors can make their results available to the community, in citable form, before we publish the edited article. We will replace this *Accepted Manuscript* with the edited and formatted *Advance Article* as soon as it is available.

You can find more information about *Accepted Manuscripts* in the [Information for Authors](#).

Please note that technical editing may introduce minor changes to the text and/or graphics, which may alter content. The journal's standard [Terms & Conditions](#) and the [Ethical guidelines](#) still apply. In no event shall the Royal Society of Chemistry be held responsible for any errors or omissions in this *Accepted Manuscript* or any consequences arising from the use of any information it contains.

1
2
3
4
5
6 Capabilities and limitations of LA-ICP-MS for depth resolved analysis of CdTe
7 photovoltaic devices.
8
9

10
11 Ana Gutiérrez-González,¹ Cristina González-Gago,¹ Jorge Pisonero,^{1*} Nicole
12 Tibbetts,² Armando Menéndez³, María Vélez¹, Nerea Bordel,¹
13
14

15
16
17 ¹ Department of Physics, University of Oviedo, Mieres and Oviedo, Spain

18
19 ² General Electric Global Research, Niskayuna, USA

20
21 ³ Energy Area (EN) - ITMA Materials Technology (Fundación ITMA),
22
23

24 Avilés, Spain
25
26
27
28
29
30
31
32
33
34
35

36 To whom correspondence should be addressed. E-mail:
37 pisonerojorge@uniovi.es
38
39
40
41
42
43
44
45
46
47
48
49
50
51
52
53
54
55
56
57
58
59
60

ABSTRACT

The analytical potential of ArF* excimer Laser Ablation Inductively Coupled Plasma Mass Spectrometry (LA-ICP-MS) is investigated for fast qualitative depth profile analysis of multi-layer CdTe Photovoltaic (PV) devices. Critical parameters (e.g. laser fluence and laser repetition rate) are evaluated and optimized to reduce the aerosol mixing from consecutive laser shots and to achieve a low penetration rate. As a result, high depth resolution (10s of nm) is demonstrated through the analyses of superficial and embedded coatings. For instance, a layer with a thickness of 100nm at a depth of 3 μ m is successfully measured. Moreover, qualitative profiles of major and minor elements obtained by LA-ICP-MS are validated using reference techniques such as Secondary Ion Mass Spectrometry (SIMS) or Glow Discharge Time of Flight Mass Spectrometry (GD-TOFMS). Additionally, the shape and morphology of the laser-induced craters, after different number of laser shots, are investigated using mechanical profilometry and Atomic Force Microscopy (AFM), respectively.

Keywords: LA-ICP-MS, depth profiling, Al-doped-ZnO (AZO) layer, multi-layers, CdTe photovoltaic devices, AFM.

INTRODUCTION

The use of photovoltaic (PV) materials based on the deposition of complex multi-elemental coatings on different substrates, and/or on the implantation of different elements/isotopes has increased during the last few years [1]. In particular, CdTe coated devices have received much attention as absorber materials for efficient, low-cost solar cells. Their advantages include high absorption coefficient, direct band-gap with nearly optimum values for solar photovoltaic, and good match of their electron affinity to CdS as a window material. Solar cell efficiencies, as high as 16% have been reported, and the maximum theoretical efficiency was estimated to be over 29% [2].

Physical properties of these innovative materials are closely related to the chemical distribution of the elements in the coatings and at the interfaces. Therefore, powerful direct-solid analytical techniques are required to achieve fast multi-elemental analysis, with low limits of detection, and high spatial resolution. In this vein, well-established analytical techniques for thin film analysis such as Auger Electron Spectroscopy (AES) [3,4,5], X-ray Photoelectron Spectroscopy (XPS) [6,7,8] or

1
2
3 Secondary Ion Mass Spectrometry (SIMS) [9,10] are commonly employed for the
4 chemical characterization of CdTe solar cells. However, these techniques require ultra-
5 high vacuum conditions and long analysis time due to low sputtering rates [11]. Glow
6 Discharge Time of Flight Mass Spectrometry (GD-TOFMS) is another technique with a
7 great potential for high depth resolved analysis (e.g. nanometric depth resolution)
8 [12,13]. This technique provides low matrix effects, fast analysis time and low limits of
9 detection ($\mu\text{g/g}$ - ng/g) [14,15]. However, samples have to fulfill specific requirements
10 on shape and dimensions, and the lateral resolution is very poor (e.g. sputtered area is
11 generally $\varnothing = 4 - 8 \text{ mm}$) [16].
12
13
14
15
16
17
18

19 On the other hand, Laser Ablation Inductively Coupled Plasma (LA-ICP-MS) is
20 a very sensitive direct solid analytical technique that operates at atmospheric pressure
21 conditions and provides high lateral resolution (\sim tens of μm) and simple sample
22 handling. LA-ICP-MS shows a great potential for depth profile analysis ($\sim\mu\text{m}$ scale),
23 but it is still not competitive against previous mentioned reference techniques
24 [17,18,19,20]. Improved depth resolution is achieved using laser beam homogenizers to
25 transform original Gaussian beam profiles into flat-top beam profiles with a
26 homogenous energy distribution across the entire laser beam [21,22]. However, non-
27 uniform ablation processes and matrix dependent melting processes that take place
28 during the interaction of the laser beam with the material might also affect the attainable
29 depth resolution [23,24,25]. Femtosecond (fs)-LA systems are able to reduce thermal
30 effects during the ablation process, but at the same time Gaussian beam profiles
31 provided by current fs laser systems produce conical crater shapes that degrade the
32 depth resolution [20]. Another key parameter affecting LA depth resolution is the
33 penetration depth per laser shot. Low laser fluence would be required to achieve
34 minimum ablation rates, but it should be considered that fractionation effects might be
35 enhanced at these conditions.
36
37
38
39
40
41
42
43
44
45
46
47

48 In this manuscript, the above operating parameters are evaluated and optimized
49 to achieve fast qualitative depth profile analysis of CdTe photovoltaic devices using
50 LA-ICP-MS. In particular, the analytical potential of a flat-top ArF* excimer LA-ICP-
51 MS is investigated for high lateral and depth resolved analysis of superficial and
52 embedded coatings. Moreover, results are compared to those obtained using reference
53 techniques for depth profile analysis, such as SIMS and GD-TOFMS.
54
55
56
57
58
59
60

EXPERIMENTAL

A Photon Machines Analyte G2 ArF* ablation system (Photon Machines, Redmond, USA) operating at the conditions summarized in Table 1 was used in these experiments. Laser ablation was performed in a HelEx two-volume ablation cell [26] that provides low aerosol washout times (2.5 orders of magnitude per second). This HelEx cell has uniform response through its square sampling area (150 mm x 150 mm) with high sensitivity, accuracy and precision. Helium cell gas (99.999% minimum purity) from Air Liquid (Oviedo, Spain) was introduced in the cell through two different inlet lines placed at the bottom part of the cell and at the internal cup, respectively. The total carrier gas was held constant at 1 L/min (0.5 L/min in the bottom cell and 0.5 L/min through the internal cup).

The detection was carried out by an Agilent 7700cx ICP-MS (Agilent Technologies, Santa Clara, USA). High purity Ar (99.999% minimum purity) from Air Liquide (Oviedo, Spain) was employed as plasma and make up gases. Operation conditions in the ICP-MS (e.g. ion optics, gas flows) were daily optimized. The ion optic was adjusted to obtain the maximum sensitivity monitoring $^7\text{Li}^+$, $^{133}\text{Cs}^+$, $^{232}\text{Th}^+$ and $^{238}\text{U}^+$ signals produced by the ablation of the standard reference material NIST 612 in raster mode. Additionally, the flow of Ar make-up gas was adjusted to keep the ratios $^{238}\text{U}^+ / ^{232}\text{Th}^+$ and $^{248}\text{ThO}^+ / ^{232}\text{Th}^+$ below 120 % and 0.5 % respectively. The calibration of the digital and analogous detectors was also daily carried out to warrant a linear response in the detection. The aerosol was transported from the ablation cell to the ICP-MS through a polytetrafluoroethylene (PTFE) tube (~ 1.5 m length and 2.5 mm i.d.).

Photovoltaic samples, which consist of an Al-doped ZnO (2wt%) (AZO) layer with a thickness of 500 nm deposited on a Si substrate, were analyzed. The AZO layers were deposited using a magnetron sputtering-up physical vapour deposition (PVD) system (ATC Orion 8HV - AJA International, USA). PVD was carried out at room temperature, pressure of 2.2mTorr and applying an rf forward power to a ceramic ZnO:Al₂O₃ (2wt%) target of 120 W.

Additionally, CdTe Photovoltaic (PV) devices were investigated for depth profiling analysis. These samples have a layer structure consisting of back metal contact followed by a CdTe layer (between 2-3 μm), a CdS layer (100 nm) and a F-SnO₂ layer (400 nm) on soda-lime. Prior to the analysis, these PV-devices were physically

1
2
3 delaminated at back metal contact / CdTe interface so the starting surface for analysis
4 was the CdTe layer.
5
6

7 Crater shapes and crater depths from sample surface were determined using a
8 mechanical step profilometer (XP1 – Ambios technology, USA), and surface roughness
9 characterization was performed by Atomic Force Microscopy (AFM) with a
10 NanotecTM microscope. In particular, AFM measurements were performed in the
11 dynamic mode using Nanosensors probes with resonance frequency 310 kHz.
12
13
14

15 RESULTS AND DISCUSSION

16 **Influence of laser fluence on the ablation process.**

17
18
19
20 Al-doped ZnO layers (500 nm) deposited on Si wafers were used as testing
21 samples due to their extremely low surface roughness (in the order of a few nm). The
22 ablation rate per laser pulse in the ZnO layer was evaluated for different laser fluences
23 (between 1.03 and 8.58 J/cm²), using a circular spot with a diameter of 65 μm. Figure 1
24 plots the depth of craters induced in the ZnO material by a single laser shot at different
25 fluences. It is observed that there is a logarithmic relationship between the ablation rate
26 per laser pulse and the laser fluence. This behavior is due to screening effects of the
27 incident radiation by the vapor/plasma plume, which are produced using moderate-to-
28 high laser output intensities and pulse lengths longer than picoseconds [27,28]. Figure 2
29 shows that at low fluence conditions (1.03 J/cm²), the interaction of the flat-beam ArF*
30 laser with the Al-doped ZnO layers results in the formation of well-defined craters with
31 a depth of about 50 nm. Additionally, re-deposition around the laser-induced crater was
32 negligible at these operating conditions.
33
34
35
36
37
38
39
40
41
42

43 Further experiments were performed increasing the number of laser shots at a
44 frequency of 1Hz. In these cases, a linear relationship was obtained between the crater
45 depth and the number of laser shots. For instance, Figure 3 shows that the AZO coating
46 (500nm) was completely ablated after 10 laser shots (e.g. average ablation rate of 50
47 nm/pulse). These results demonstrate the analytical potential of LA-ICP-MS to achieve
48 depth profile analysis with high depth resolution (10s of nm). Nevertheless, it should be
49 highlighted that the ablation rate is greatly affected by material optical properties and
50 laser wavelength.
51
52
53
54
55
56
57
58
59
60

Qualitative depth profile analysis of multi-layer CdTe photovoltaic devices.

The analytical potential of LA-ICP-MS was investigated for depth profile analysis of multi-layer CdTe photovoltaic devices. In particular, the effect of the spot size and laser frequency on the achieved depth resolution was evaluated and optimized. The laser fluence was fixed at the minimum value ($\sim 1\text{Jcm}^{-2}$) for each analysis to ensure a minimum penetration depth per laser pulse. During the first 30 seconds, ICP-MS background ion signals were measured, and then, the different layers were ablated. The external CdTe layer was analyzed through the measurement of $^{111}\text{Cd}^+$ and $^{125}\text{Te}^+$ ion signals. Afterwards, the CdS layer was resolved with the $^{34}\text{S}^+$ signal and the SnO_2 layer was monitored by $^{119}\text{Sn}^+$ ion signal. Finally, the soda-lime glass substrate was identified through the detection of the $^{23}\text{Na}^+$ ion signal. Figure 4(a,b) shows the qualitative depth profiles of the multi-layer CdTe photovoltaic cell, obtained at 10 Hz for two different laser spot diameters ($65\mu\text{m}$ and $160\mu\text{m}$, respectively). In both cases, the different layers can be distinguished but they are not completely resolved. Mixing of coatings is more pronounced using the laser spot diameter of $160\mu\text{m}$ due to higher amount of ablated material per laser shot. Therefore, the spot size diameter of $65\mu\text{m}$ was chosen to achieve a better relation between sensitivity and depth resolution.

In order to improve the depth resolution, lower laser repetition rates were also evaluated to further avoid aerosol mixing during aerosol transport. Figure 5 shows the qualitative depth profiles of multi-layer CdTe photovoltaic cells, obtained at lower laser frequencies, 5 Hz and 1 Hz, using a spot size of $65\mu\text{m}$ of diameter. It is observed that at the interfaces between the different layers, ion signals have faster decays using lower laser frequencies. In a supplemental Figure, qualitative depth profiles obtained at 5Hz and at 1 Hz are plotted removing the Sn^+ ion signal. This Figure clearly shows that working at 1 Hz it is possible to avoid the overlapping between the S^+ ion signal and the Na^+ ion signals that represents the glass substrate. These results indicate that the use of minimum repetition rates leads to reducing signal mixing, improving depth resolution.

At a laser repetition rate of 1 Hz, ion signal oscillations follow the laser frequency due to the fast wash out of the ablation cell. Nevertheless, qualitative depth profiles can be mathematically treated using a smoothing function after ion signal integration of each laser pulse, in order to get a better defined depth profile. Figure 6 shows the smoothed qualitative depth profile obtained for multi-layer CdTe PV using

1
2
3 the LA-ICP-MS at 1 Hz. All the layers are clearly resolved, even the thin CdS layer
4 with a thickness of 100nm. Figure 6 also shows the detection of a residual thin Mo layer
5 from the back metal contact on the surface of the sample.
6
7

8
9 Figure 7 shows the qualitative depth profiles obtained for the same multi-layer
10 CdTe PV samples using reference technique such as GD-TOFMS and SIMS [12]. It
11 should be highlighted that qualitative depth profiles obtained by LA-ICP-MS were in
12 good agreement with those obtained by GD-TOFMS and SIMS. These results show that
13 LA-ICP-MS is able to provide fast depth profile analysis with relatively high depth
14 resolution. Nevertheless, the use of low penetration rates and small laser-induced crater
15 diameters originates the ablation of very small amounts of material that produce a fast
16 transient signal. Sequential mass analysers, such as the quadrupole (Q), might limit the
17 number of monitored analytes per laser pulse due to spectral skew problems [26].
18 Therefore, fast mass analysers such as TOFMS could be recommended to improve
19 multielemental depth profiling capabilities of this technique.
20
21
22
23
24
25
26

27 28 **Laser-induced crater shape and morphology.** 29

30 Ablation process at 1 Hz was investigated in more detail during the analysis of
31 multi-layer CdTe PV devices. For this purpose, shape and morphology of the laser-
32 induced craters were measured at different depths. Figure 8(a,b) shows the crater
33 profiles measured after different number of laser shots, using two spot diameters, 65 μ m
34 and 160 μ m, respectively. The average penetration depth was found to be a function of
35 the ablated material and number of laser shots, but it was independent of the spot size.
36 Crater depth was about 1.2 μ m (middle of the CdTe layer) after 10 shots, providing an
37 average ablation rate of 120nm/pulse in this material, which is significantly larger than
38 that obtained for the AZO layers. Laser-induced crater depth was about 2.5 μ m (middle
39 of CdS layer) after 22 shots. At this point, it should be mentioned that $^{34}\text{S}^+$ ion signal
40 (Figure 5b) was detected during several laser shots, indicating an average ablation rate
41 of the CdS layer (100nm of thickness) below 50nm/pulse. Finally, a crater depth of
42 about 3 μ m (middle of SnO₂ layer) is measured after 33 shots, which results in an
43 average ablation rate of about 50nm/pulse in this material.
44
45
46
47
48
49
50
51
52
53

54 It was observed that crater profiles were not completely flat (e.g. more ablation
55 was observed at the edge of the crater and some roughness was found at the crater
56 bottom). The convexity of the crater was enhanced at increasing number of pulses, but it
57
58
59
60

1
2
3 decreased when reaching the SnO₂ layer, highlighting the influence of the material
4 composition on the ablation process.
5
6

7 The morphology of the laser-induced craters was investigated using an atomic
8 force microscope (AFM). In particular, the laser-induced roughness was measured at the
9 bottom of the 160 μm spots. Figure 9 shows the AFM images (scanning area of 10μm x
10 10μm) after different number of laser shots (e.g. different layers of the CdTe PV
11 device). At the surface of the CdTe device (before any ablation process) a grain-
12 structure was observed with an average roughness of about 90 nm (root mean square
13 (RMS) value). Once the CdTe layer was partially ablated, the grain-structure
14 disappeared and some melting processes were detected. In that case, the average
15 roughness measured at the bottom of the laser-induced crater was improved to about
16 30nm. This value remained constant after 22 laser shots (CdS layer) but it significantly
17 changed when the SnO₂ layer was ablated. At this layer, the average roughness was
18 reduced to about 6nm, which is also the value measured at the glass substrate (after 100
19 laser shots). Laser induced roughness and crater shape are factors that have a great
20 influence on the depth resolution that can be achieved by LA-ICP-MS but it is observed
21 that they mainly depend on the laser-matter interaction (e.g. composition of the
22 coating).
23
24
25
26
27
28
29
30
31
32
33

34 CONCLUSIONS

35
36 The analytical capabilities of a flat-top beam ArF* excimer ns-LA-ICP-MS
37 system have been investigated for fast qualitative depth profile analysis of multi-layer
38 CdTe Photovoltaic (PV) devices. The influence of the laser fluence on the penetration
39 rate has been initially evaluated using an AZO layer with an original highly-smooth
40 surface. A minimum penetration rate of ~50nm per laser pulse has been achieved in a
41 well-defined laser-induced crater. However, dependence of laser ablation rate on the
42 layer composition significantly affects the depth resolution that can be achieved using
43 LA-ICP-MS for the depth profile analysis of innovative materials.
44
45
46
47
48
49
50

51 In this study, qualitative depth profiles of the multi-layer CdTe PV device,
52 containing thin layers (~ 100 nm), were successfully measured and in agreement with
53 profiles obtained by other reference techniques such as GD-TOFMS and SIMS.
54 Moreover, it has been observed that depth resolution of the qualitative depth profiles
55 obtained by this LA-ICP-MS system is negatively affected by different parameter,
56
57
58
59
60

1
2
3 including convex laser-induced crater shapes, large laser spot sizes and high laser
4 repetition rates. Additionally, laser-induced roughness measured at the bottom of the
5 crater has been found to be strongly dependent on the material composition of the
6 ablated layer.
7
8

9 10 ACKNOWLEDGMENTS

11
12 Financial support from Photon-Machines and Teledyne CETAC through project
13 FUIO-EM-031-13, and from “Plan Nacional de I + D + I” (Spanish Ministry of Science
14 and Innovation and Feder Programme) through MAT2010-20921-C02-02 and FIS2008-
15 06249, are gratefully acknowledged. Dustin Ellis, Laurie LeTarte and Vincent S.
16 Smentkowski from GE-GRC are thanked for useful discussion and other supporting
17 characterization results which are not summarized here. Ana Luisa Martinez from
18 Fundación ITMA is thanked for the support on the ZnO samples preparation.
19
20
21
22
23
24
25
26
27
28
29
30
31
32
33
34
35
36
37
38
39
40
41
42
43
44
45
46
47
48
49
50
51
52
53
54
55
56
57
58
59
60

TABLES

Table 1: Operating conditions.

Laser System	
Wavelength	193 nm
Pulse duration	4 ns
Repetition rate	1-10 Hz
Fluence	1.03-8.58 J/cm ²
Gas cell	He 1 L/min
ICP-MS	
RF Power	1600 W
Plasma gas	Ar 15 L/min
Carrier gas	Ar 1 L/min
Auxiliary gas	Ar 1 L/min
Integration time per isotope	10 ms
Samples	
NIST 612	⁷ Li, ¹³³ Cs, ²³² Th, ²³⁸ U, ²⁴⁸ ThO
CdTe PV device	²³ Na, ²⁷ Al, ³⁴ S, ⁹⁵ Mo, ¹¹¹ Cd, ¹¹⁹ Sn, ¹²⁵ Te
ZnO (AZO)	²⁹ Si, ⁶⁶ Zn

1
2
3
4
5
6
7
8
9
10
11
12
13
14
15
16
17
18
19
20
21
22
23
24
25
26
27
28
29
30
31
32
33
34
35
36
37
38
39
40
41
42
43
44
45
46
47
48
49
50
51
52
53
54
55
56
57
58
59
60

LEGEND OF FIGURES

Figure 1. Crater depth measured on AZO layers as a function of laser fluence, based on single-shot experiments. The curved solid line represents the logarithmic function that best fits between data points. RSD (about 20%) was calculated from external reproducibility (3 analyses) and also considering the uncertainty from induced roughness at each crater bottom.

Figure 2. Cross section of the crater obtained on AZO layers after single laser shot at 1.03 J/cm^2 .

Figure 3. Qualitative depth profile of the Al-doped ZnO layer (thickness 500nm) deposited on a Si substrate, obtained using 1 Hz and a circular laser spot with a diameter of $65 \mu\text{m}$.

Figure 4. Qualitative depth profiles of multi-layer CdTe photovoltaic cells, obtained using 10 Hz and a circular laser spot with a diameter of: (a) $65 \mu\text{m}$; (b) $160 \mu\text{m}$.

Figure 5. Qualitative depth profiles of multi-layer CdTe photovoltaic cells, obtained for a circular laser spot diameter of $65 \mu\text{m}$ at a laser frequency of: (a) 5 Hz; (b) 1 Hz.

Figure 6. Smoothed qualitative profile obtained for multi-layer CdTe PV using a laser frequency of 1 Hz and a circular spot with a diameter of $65 \mu\text{m}$.

Figure 7. Qualitative depth profiles of multi-layer CdTe photovoltaic cells, obtained using: (a) GD-TOFMS; (b) SIMS. With permission from [C. Gonzalez-Gago, J. Pisonero, N. Bordel, A. Sanz-Medel, N. J. Tibbetts and V. S. Smentkowski, J. Vac. Sci. Technol, 2013, DOI:10.1116/1.4824164]

Figure 8. Crater profiles measured in the CdTe PV sample using a profilometer, after different number of laser shots (10, 22 and 33) operated at 1Hz. Crater profiles obtained for two spot sizes with $65 \mu\text{m}$ and $160 \mu\text{m}$ of diameter. The number of laser shots was selected to reach each of the different layers of the CdTe PV device.

Figure 9. AFM images (top view) with a scan size of $10 \mu\text{m} \times 10 \mu\text{m}$: a) surface of the photovoltaic device; b) CdTe layer (after 10 shots); c) CdS layer (after 22 shots);

d) SnO₂ layer (after 33 shots); e) substrate (after 100 shots). Laser was operated at 1Hz. Laser induced roughness is indicated for each layer.

Supplemental Figure: Qualitative depth profiles of multi-layer CdTe photovoltaic cells, obtained for a circular laser spot diameter of 65 μm at a laser frequency of: (a) 5 Hz; (b) 1 Hz. In particular, Sn⁺ ion signal that represents the SnO₂ layer has been removed to show in more detail overlapping between S⁺ and Na⁺ ion signals.

REFERENCES:

[1] T. Markvart and L. Castañer, *Solar Cells: Materials Manufacture and Operation*, Elsevier Science & Technology, Oxford, 2005.

[2] K. D. Dobson, I. Visoly-Fisher, G. Hodes, D. Cahen, *Solar Energy Materials & Solar Cells*, 2000, **62**, 295-325.

[3] A. Martel, F. Caballero-Briones, A. I. Oliva, R. Castro-Rodríguez, A. Iribarren, P. Bartolo-Pérez and J. L. Peña, *Physica status solidi*, 2000, **220**, 261-267.

[4] E. Barojas, R. Silva-González, J. Pantoja-Enríquez, *Solar Energy Materials & Solar Cells*, 2006, **90**, 2235-2240.

[5] J. Pantoja-Enríquez, E. Gómez-Barojas, R. Silva-González and U. Pal, *Solar Energy Materials & Solar Cells*, 2007, **91**, 1392-1397.

[6] K.D. Rogers, J.D. Painter, M.J. Healy, D.W. Lane and M.E. Ozsan, *Thin Solid Films*, 1999, **339**, 299-304

[7] X. Wu, S. Asher, D. H. Levi, D. E. King, Y. Yan, T. A. Gessert, and P. Sheldon, *J. Appl. Phys.*, 2001, **89**, 4564-4569.

[8] P. Boieriu, R. Sporcken, A. Adriaens, Y. Xin, N.D. Browning and S. Sivananthan, *Nucl. Instr. and Meth. in Phys. Res.*, 2000, **161-163**, 975-979.

[9] M. Emziane, K. Durose, D.P. Halliday, N. Romeo and A. Bosio, *Thin Solid Films*, 2006, **511-512**, 66-70.

[10] O. Koudriavtseva, A. Morales-Acevedo, Y. Kudriavtsev, S. Gallardo, R. Asomoza, R. Mendoza-Perez, J. Sastre-Hernandez and G. Contreras-Puente. *Appl. Surf. Sci.*, 2008, **255**, 1423-1426.

[11] R. Escobar-Galindo, R. Gago, A. Lousa and J. M. Abella, *Trends Anal. Chem.*, 2009, **28**, 494-505.

[12] J. Pisonero, N. Bordel, C. Gonzalez de Vega, B. Fernández, R. Pereiro and A. Sanz-Medel, *Anal. and Bioanal. Chem.*, 2013, **405**, 5655-5662.

[13] C. Gonzalez-Gago, J. Pisonero, N. Bordel, A. Sanz-Medel, N. J. Tibbetts and V. S. Smentkowski, *J. Vac. Sci. Technol.*, 2013, DOI:10.1116/1.4824164

[14] L. Lobo, B. Fernandez, R. Pereiro, N. Bordel, E. Demenev, D. Giubertoni, M. Bersani, P. Honicke, B. Beckhoff and A. Sanz-Medel, *J. Anal. At. Spectrom.*, 2011, **26**, 542-549.

-
- 1
2
3
4
5
6 [15] J. Pisonero, A. Licciardello, A. Hierro-Rodríguez, C. Quirós, A. Sanz-Medel and
7 N. Bordel, *J. Anal. At. Spectrom.*, 2011, **26**, 1604-1609.
- 8 [16] J. Pisonero, B. Fernandez and D. Günther, *J. Anal. At. Spectrom.*, 2009, **24**, 1145–
9 1160.
- 10 [17] J. Pisonero and D. Gunther, *Mass Spectrometry Reviews*, 2008, **27**, 609-623.
- 11 [18] D. Bleiner, A. Plotnikov, C. Vogt, K. Wetzig and D. Günther, *Fresenius J Anal*
12 *Chem.*, 2000, **368**, 221-226.
- 13 [19] L. Balcaen, J. Lenaerts, L. Moens and F. Vanhaecke, *J. Anal. At. Spectrom.*, 2005,
14 **20**, 417-423.
- 15 [20] J. Pisonero, J Koch, M. Walle, W. Hartung, N. D. Spencer and D. Günther, *Anal.*
16 *Chem.*, 2007, **79**, 2325-2333.
- 17 [21] D. Günther, R. Frischknecht, CA. Heinrich and HJ, Kahlert, *J Anal At Spectrom.*,
18 1997, **12**, 939–944.
- 19 [22] M. Guillon, I. Horn, D. Günther. *J. Anal. At. Spectrom.*, 2002, **17**, 8–14.
- 20 [23] J. Mikova, J. Kosler, H. P. Longerich, M. Wiedenbeck and J. M. Hanchar, *J. Anal.*
21 *At. Spectrom.*, 2009, **24**, 1244–1252.
- 22 [24] M. G. Babechuk, B. S. Kamber, A. Greig, D. Canil and J. Kodolanyi, *Geochim.*
23 *Cosmochim. Acta.*, 2010, **74**, 1448–1470.
- 24 [25] D. Bleiner, Z. Chen, D. Autrique and A. Bogaerts, *J. Anal. At. Spectrom.*, 2006, **21**,
25 910–921.
- 26 [26] W. Müller, M. Shelley, P. Miller and S. Broude, *J. Anal. At. Spectrom.*, 2009, **24**,
27 209-214.
- 28 [27] D. Bauerle. *Laser Processing and Chemistry*, Springer-Verlag, 2011.
- 29 [28] M. Stafe, C. Negutu, N.N. Puscas, I.M. Popescu, *Rom. Reports in. Physics*, 2008,
30 **62**, 758-770.
- 31
32
33
34
35
36
37
38
39
40
41
42
43
44
45
46
47
48
49
50
51
52
53
54
55
56
57
58
59
60

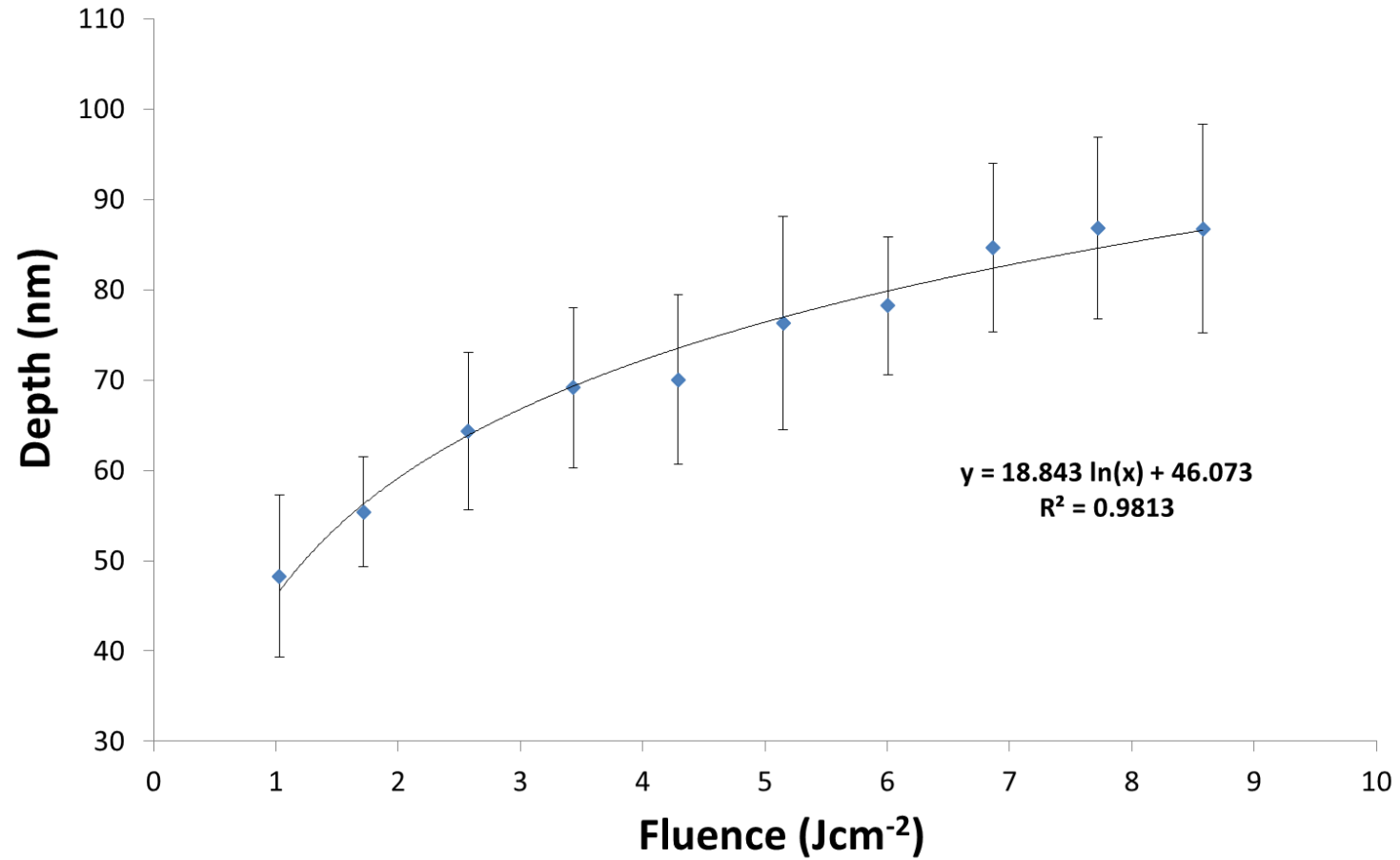


Figure 1

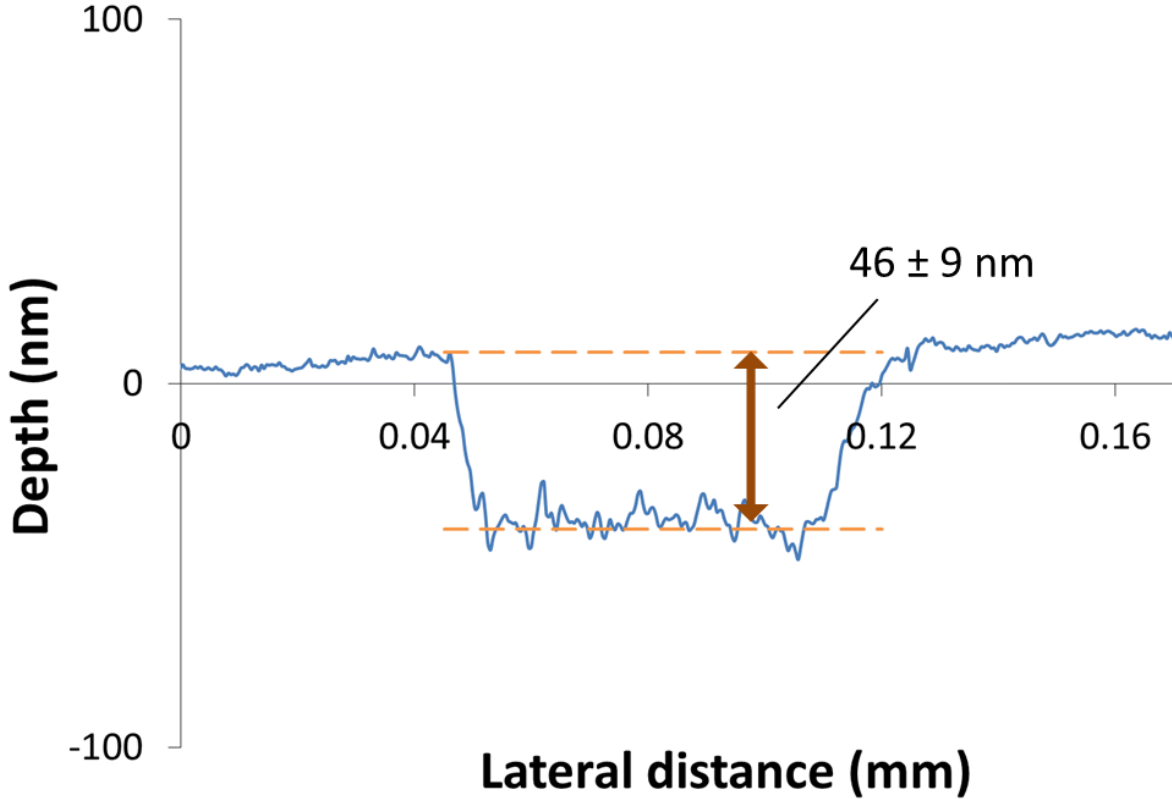


Figure 2

1
2
3
4
5
6
7
8
9
10
11
12
13
14
15
16
17
18
19
20
21
22
23
24
25
26
27
28
29
30
31
32
33
34
35
36
37
38
39
40
41
42
43

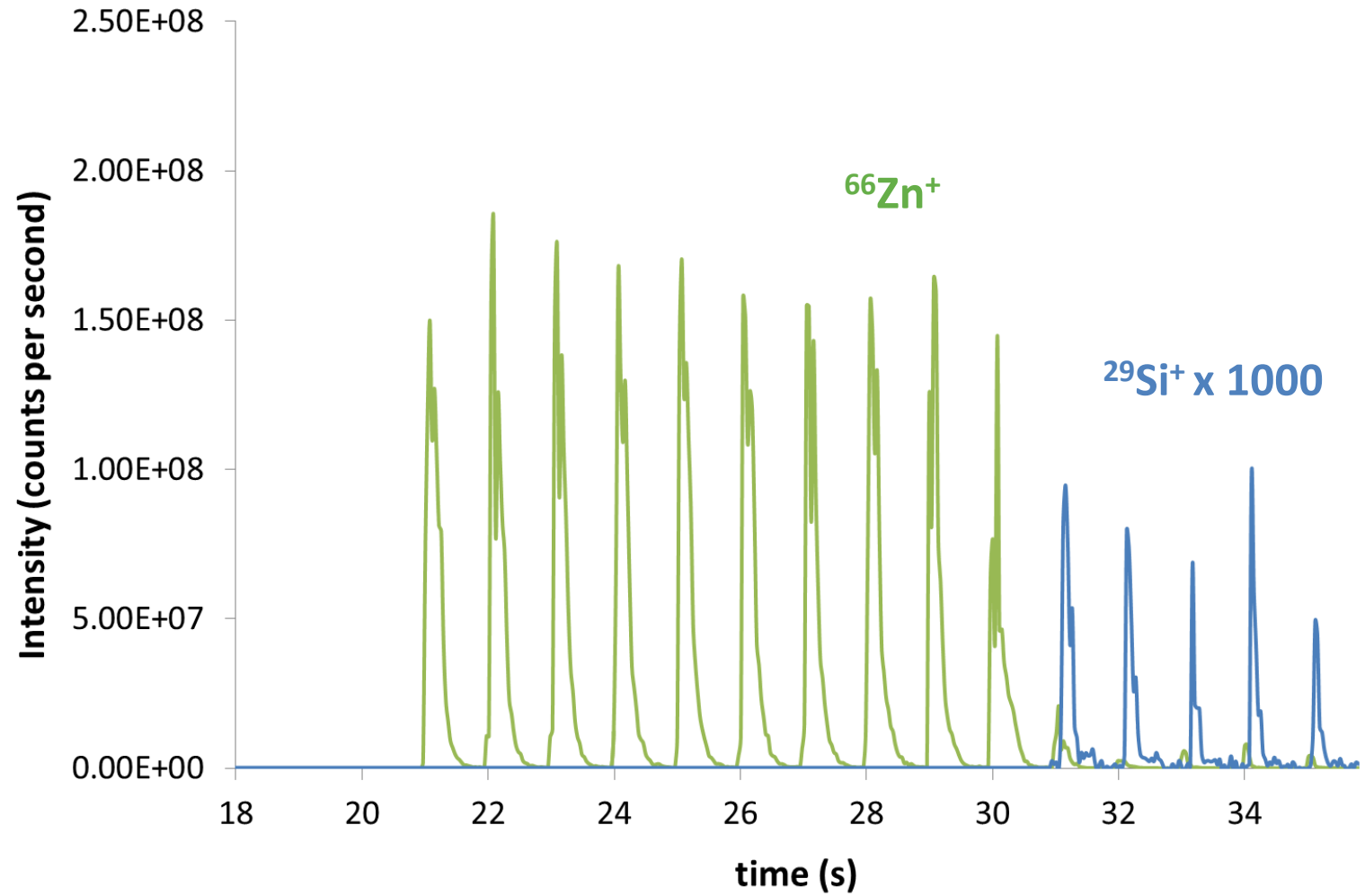


Figure 3

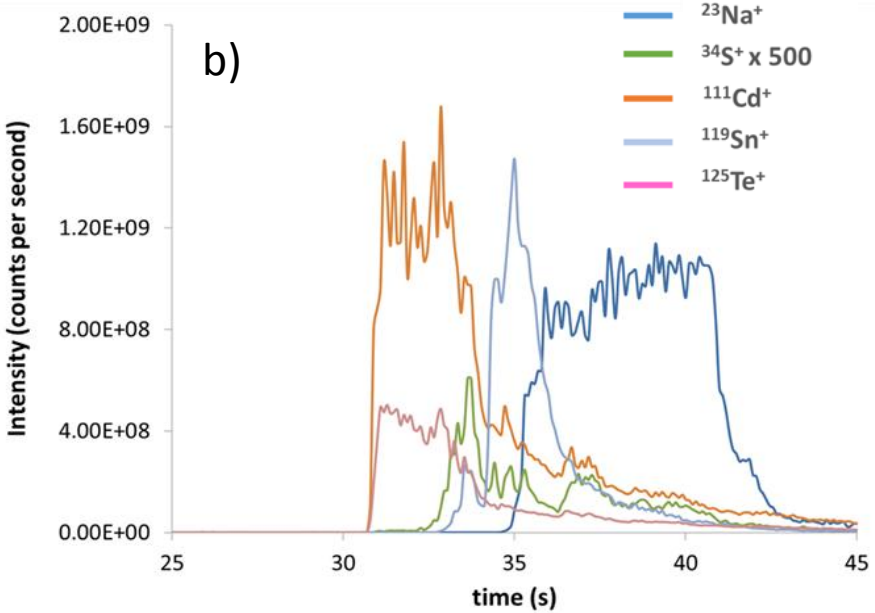
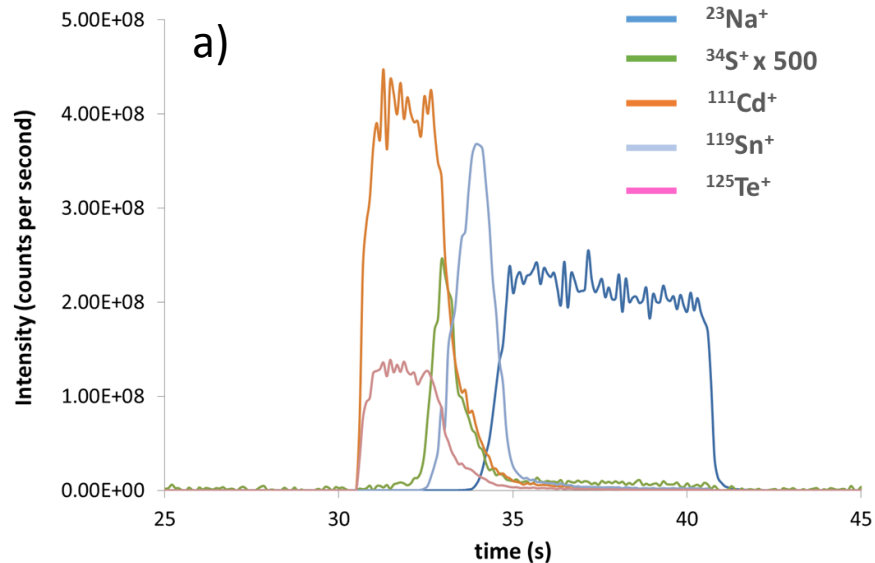


Figure 4

1
2
3
4
5
6
7
8
9
10
11
12
13
14
15
16
17
18
19
20
21
22
23
24
25
26
27
28
29
30
31
32
33
34
35
36
37
38
39
40
41
42
43

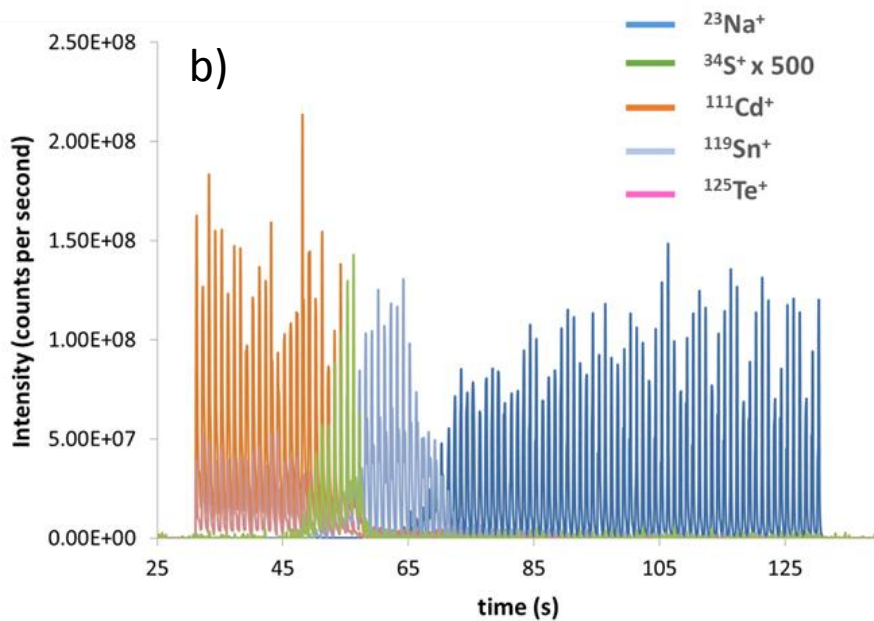
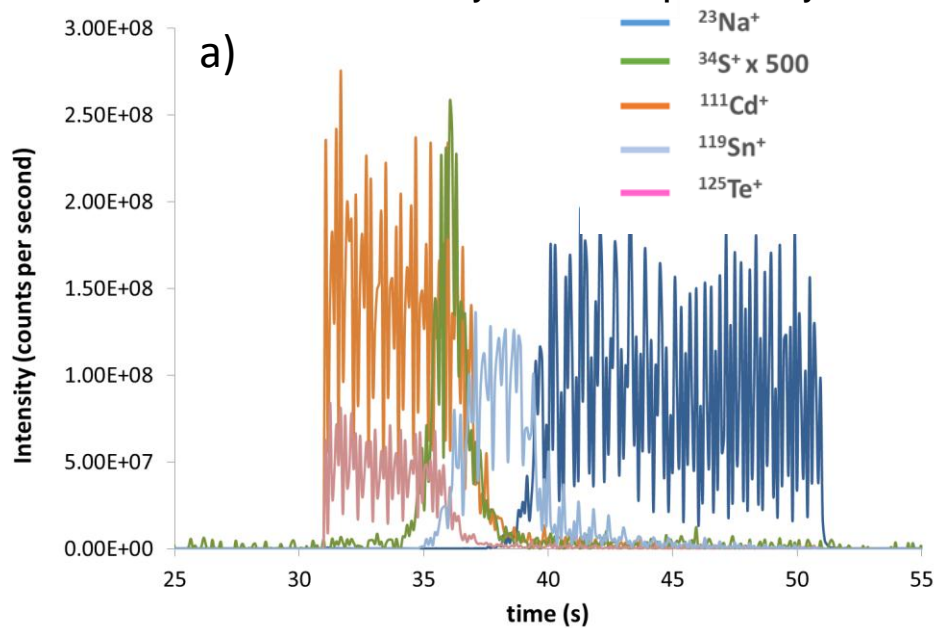


Figure 5

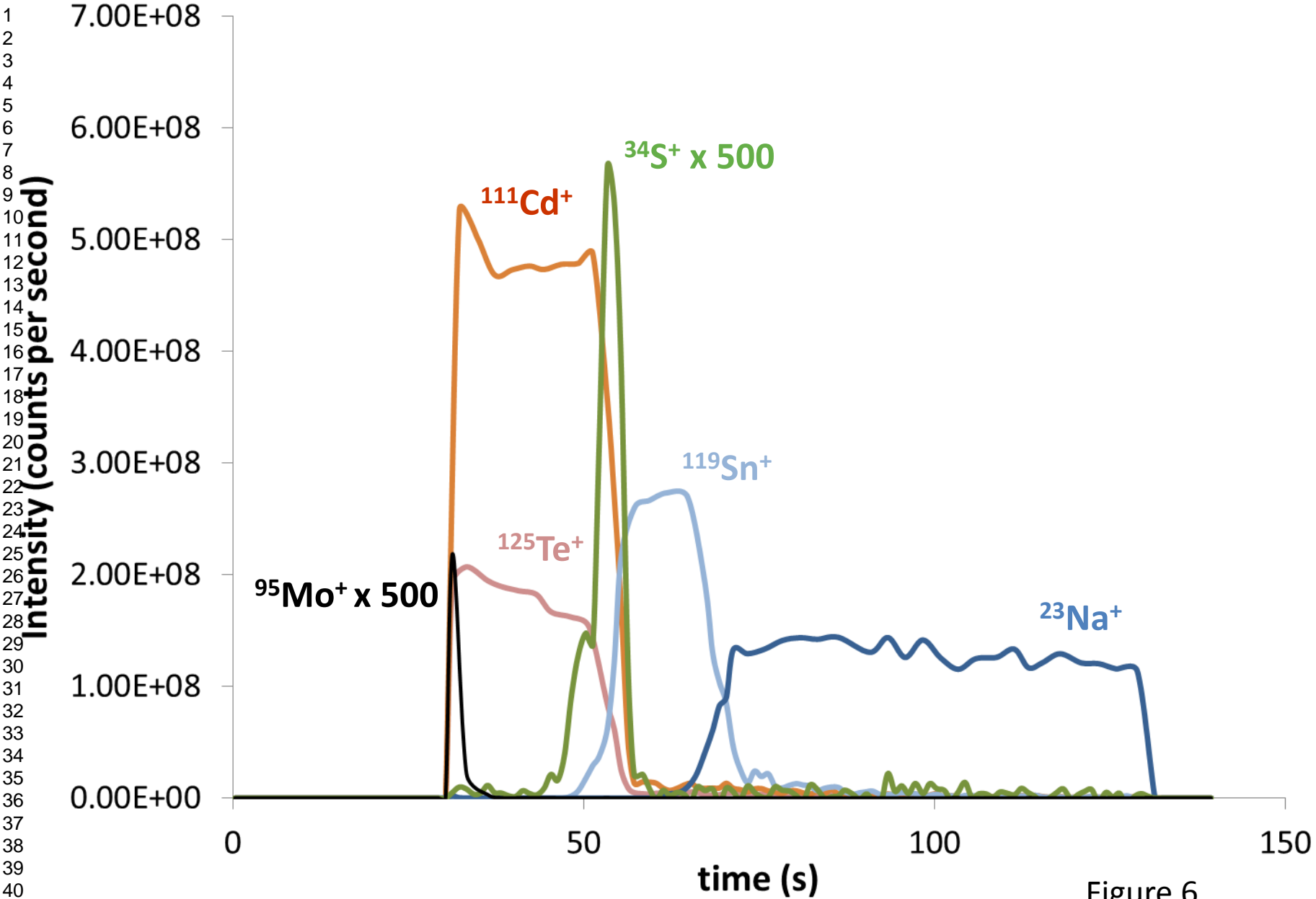


Figure 6

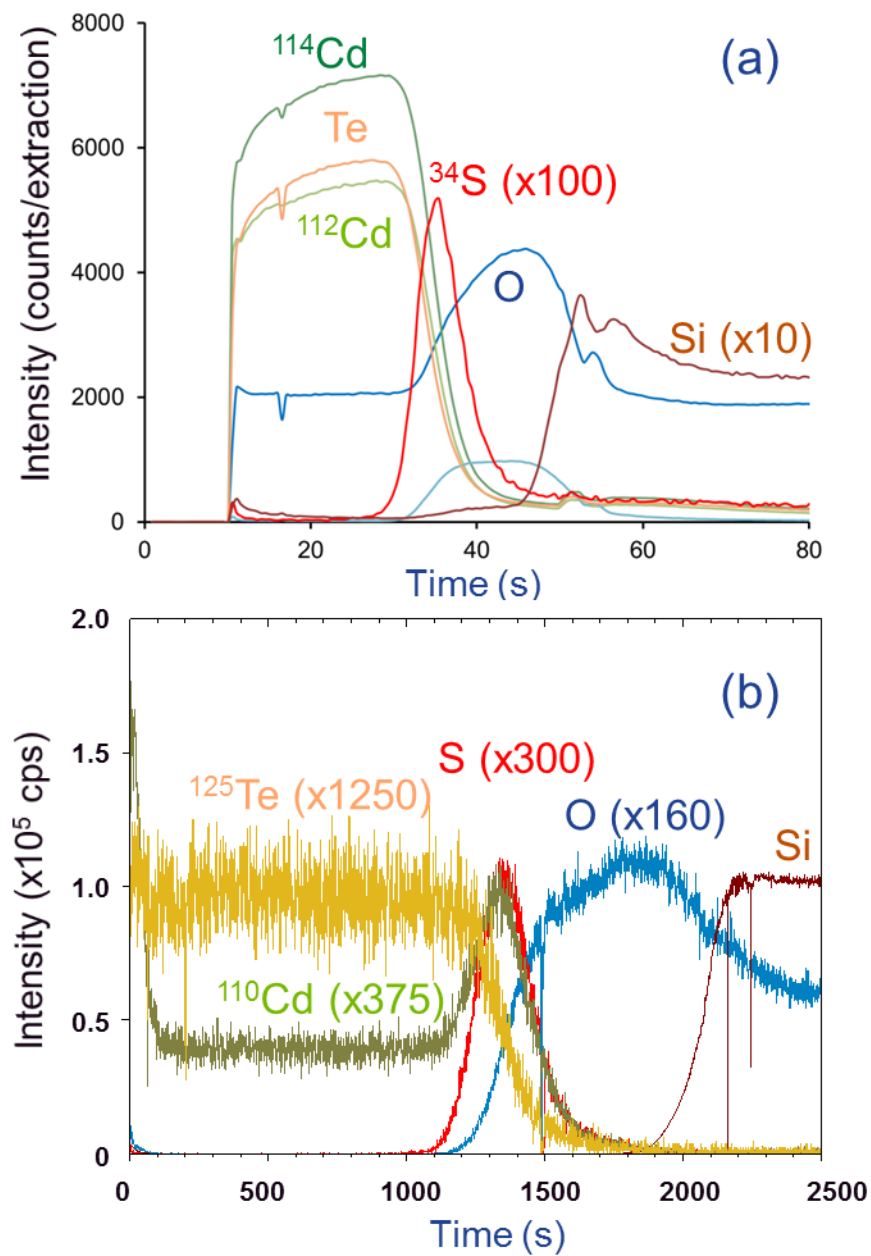


Figure 7

1
2
3
4
5
6
7
8
9
10
11
12
13
14
15
16
17
18
19
20
21
22
23
24
25
26
27
28
29
30
31
32
33
34
35
36
37
38
39
40
41
42
43

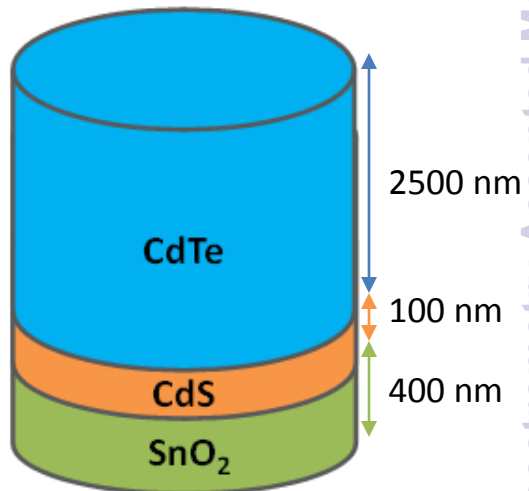
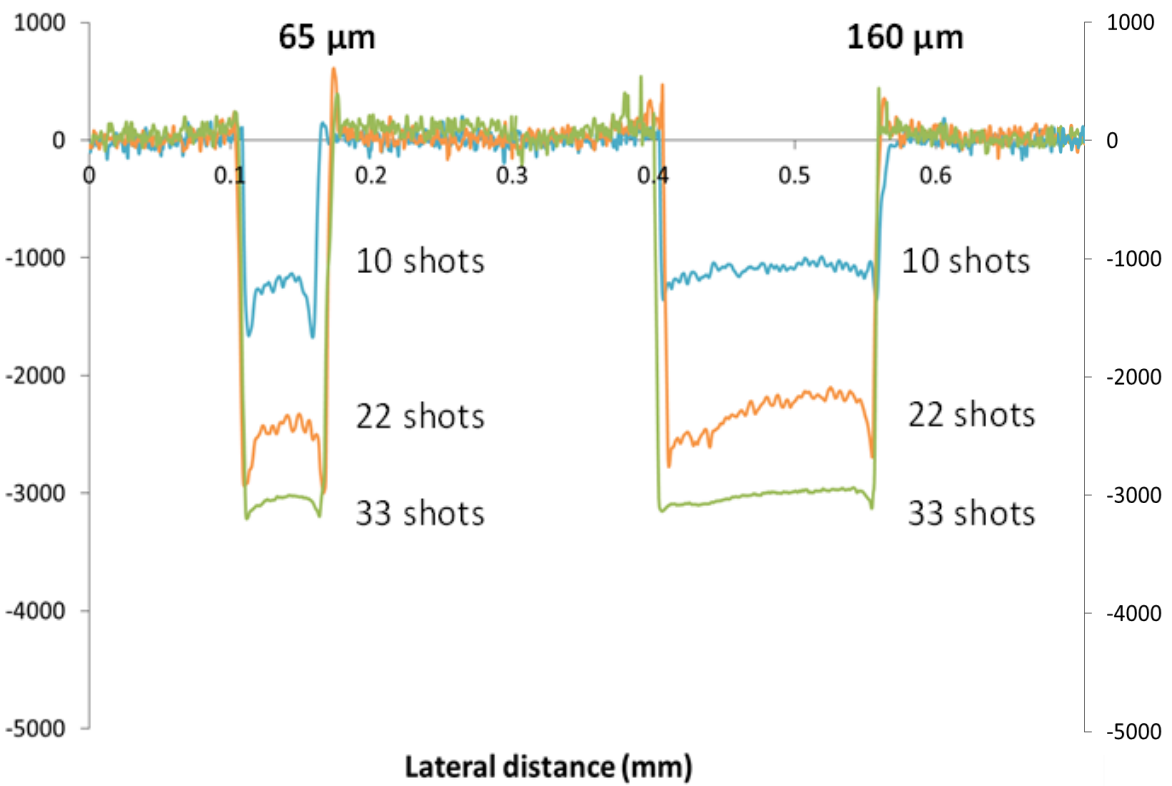


Figure 8

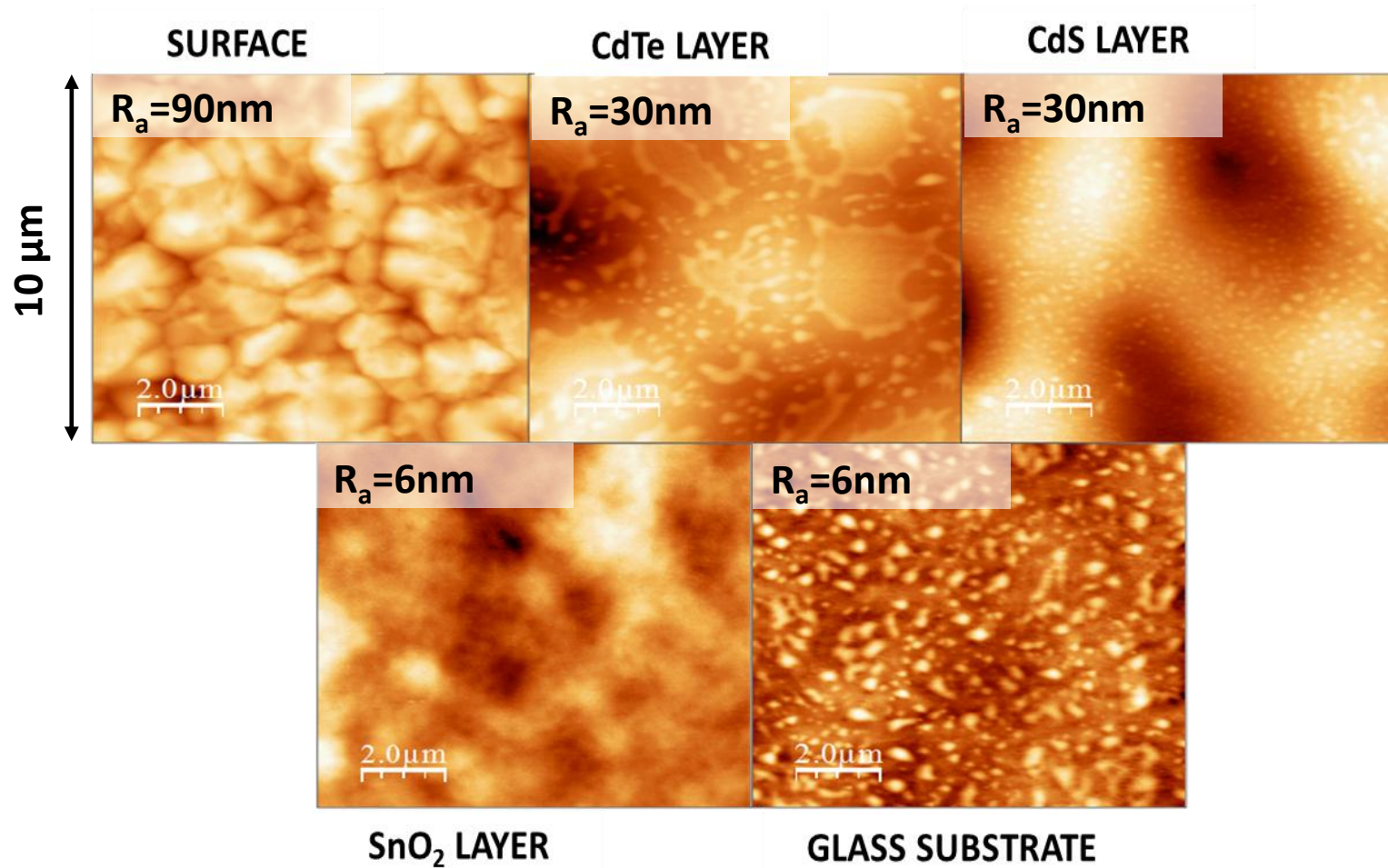
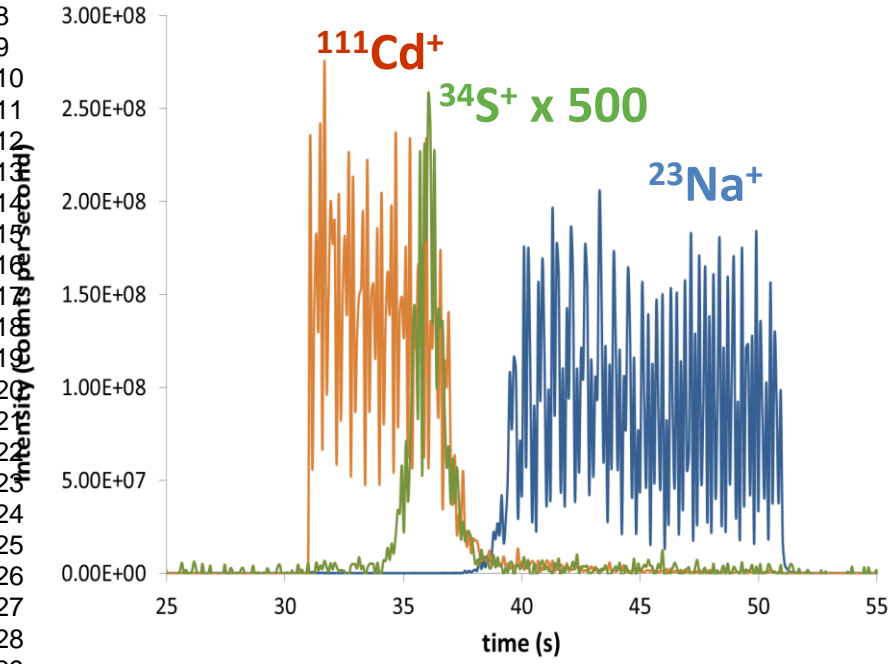


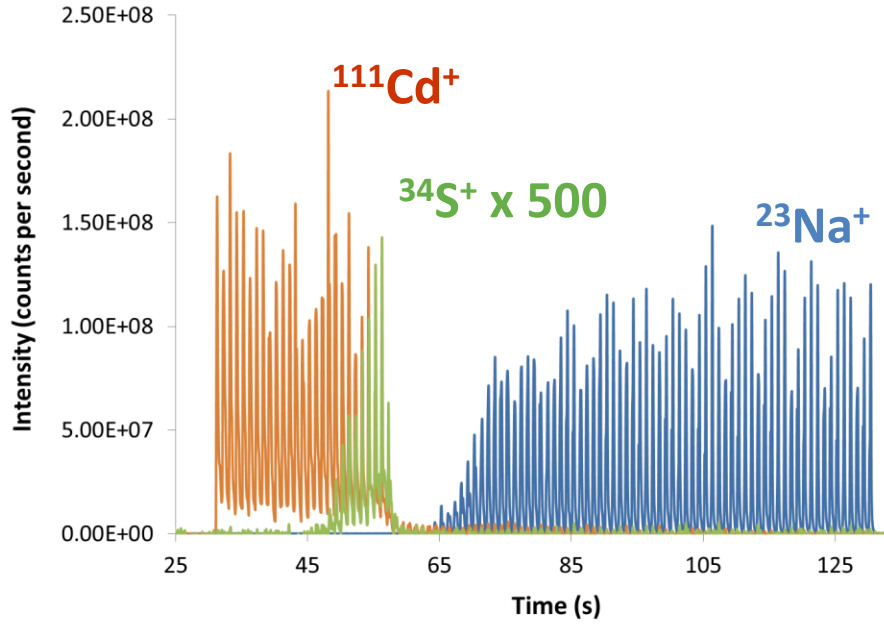
Figure 9

1
2
3
4
5
6
7
8
9
10
11
12
13
14
15
16
17
18
19
20
21
22
23
24
25
26
27
28
29
30
31
32
33
34
35
36
37
38
39
40
41
42
43

a)



b)



Supplemental
Figure